Dyes and Pigments 207 (2022) 110686

Contents lists available at ScienceDirect

Dyes and Pigments

journal homepage: www.elsevier.com/locate/dyepig

Novel silicon phthalocyanine photosensitizers containing carboxylic acid based axial anchoring groups: Electrochemistry, spectroelectrochemistry, and dye sensitized solar cell performance

Gülşah Gümrükçü Köse [a,*], Gülnur Keser Karaoğlan [a], Yaren Erdağ Maden [b], Atıf Koca [b,**]

[a] Yıldız Technical University, Arts and Science Faculty, Chemistry Department, 34220, Istanbul, Turkey
[b] Marmara University, Engineering Faculty, Chemical Engineering Department, Istanbul, Turkey

ARTICLE INFO

Keywords:
Dye sensitized solar cell
Phthalocyanine
Carboxylic acid
Spectroelectrochemistry
Electrochemistry

ABSTRACT

In this study, two novel silicon phthalocyanines (SiPc) having axial anchoring groups (**3**: SiPc carrying bis-dibutyl phenoxy acrylic acid and **5**: SiPc carrying bis-dibutyl phenoxy carboxylic acid) are synthesized as the photosensitizers of dye sensitized solar cells (DSSCs). The obtained novel photosensitizers are elucidated by using ^{1}H NMR, MALDI-TOF, FT-IR, UV–Vis spectroscopy, and elemental analysis. Moreover, the electrochemistry of SiPcs is investigated with voltametric and in-situ spectroelectrochemical analysis. Both SiPcs illustrate similar two reductions and one oxidation Pc based redox processes. In-situ spectroelectrochemical results support the Pc based characters of the voltametric responses. The chromaticity diagrams and optical responses of the anionic and cationic moieties are recorded with the in-situ spectroelectrochemistry to determine the viability of them for various photoelectrochemical usage. Finally, SiPcs are investigated as dyes in DSSCs in order to investigate the influence of bis-dibutyl phenoxy acrylic acid and bis-dibutyl phenoxy carboxylic acid anchoring groups to the photovoltaic performance of SiPcs. DSSCs sensitized with SiPc (**3**) and SiPc (**5**) illustrate good photovoltaic performance with 1.48 and 1.99 mA/cm^2 short circuit current density, 0.751 and 0.657 V open circuit potential, 0.52 and 0.57 fill factor, and 0.57% and 0.75% power conversion efficiency respectively.

1. Introduction

Increasing demands for global energy and electronic materials together with technological advances necessitates energy transformation today. Although many industrial and technological studies are carried out for this purpose, one of these studies is dye-sensitized solar cells (DSSCs) in the field of photovoltaic technology. Efficiency in DSSCs depends on the counter electrode, photoanode, the formation of sensitizers with the electrolyte and their compatibility in operating performance [1]. Phthalocyanines (Pcs) with high thermal, chemical and light stability are very important macrocyclic compounds. Multi-electron and reversible redox activity of metallophthalocyanines (MPcs) are basic requirements for the functional materials of various electrochemical applications, such as, catalytic [1,2], sensing [3,4] and electrochromic [5,6] applications. The functionally of MPcs could be tailored by altering the metal center and substituent environments. For instance, substituting the MPcs with suitable anchoring substituents can open a way for their usage as dyes in DSSCs. So far, many functional phthalocyanines were examined as photosensitizers in DSSCs [7–10] due to their excellent light absorption in the visible and near-IR (Q band) regions in addition to their excellent redox activities, physical and chemical stability. These features of the MPcs may be manipulated by altering the number, type and substituting position of them on the Pc ring. Nonperipheral, peripheral and axial positions for the anchoring groups considerably influence MPcs functionalities in addition to the influence of the metal center of MPcs. New studies on the preparation of dyes for DSSCs are generally concentrated on the developing novel phthalocyanines having efficient absorption of the wide range of the light spectrum and strong anchoring to the TiO_2 semiconductor surface of the photoelectrode of the DSSCs [10,11]. Among phthalocyanine based DSSCs, zinc(II)phthalocyanines (ZnPc) having different substituent environments were frequently studied due to their suitable electrochemical and optical features [7,8,12–14]. MPc based studies represented that the substituent environment and variation of the

* Corresponding author.
** Corresponding author.
E-mail addresses: ggumruk@yildiz.edu.tr (G. Gümrükçü Köse), akoca@marmara.edu.tr (A. Koca).

https://doi.org/10.1016/j.dyepig.2022.110686
Received 31 May 2022; Received in revised form 18 August 2022; Accepted 19 August 2022
Available online 29 August 2022

anchoring moieties significantly affect the DSSC efficiency [14–16]. In our previous paper, we have reported photovoltaic performance of tetra-4-carboxyethylphenoxy substituted TiOPc, CoPc, ZnPc and H_2Pc having four anchoring carboxyl groups and achieved 2.9%, 3.3%, 1.02% and 2.2% of power conversion efficiencies respectively [17]. In addition to the frequently used peripherally and nonperipherally anchoring groups on the Pc ring, Al^{3+} and Si^{4+} as the metal core in the center of Pc rings containing axial anchoring groups are rarely preferred as dyes for DSSCs [10,11,18–20]. Li et al. summarized MPcs based dyes in DSSCs bearing axial anchoring groups and compared with those bearing peripherally and nonperipherally anchoring groups [21]. They reported that in addition to the type, number and position of the anchoring groups, the length of the anchoring groups, the electron withdrawing/donating natures of them, and the peak number and position of the redox processes considerably influenced the performance of the dyes [21]. Two non-aggregated silicon(IV) phthalocyanine compounds bearing two terephthalic and two carboxyphenylcyanoacrylic axial anchoring moieties were synthesized and tested as dyes in DSSCs by Sastre-Santos et al. and power conversion efficiency (PCE) of 0.53 and 0.77% were reported [19]. Güzel et al. investigated the performance of two SiPc bearing electron-withdrawing pyridine based anchoring moieties and reported the efficiency, J_{sc}, V_{oc} and FF as 0.53%, 1.205 mA cm^{-2}, 0.612 V, and 0.72, respectively [20]. In another study, PCE, J_{sc}, V_{oc} and FF values of 0.84, 2.41 mA cm^{-2}, 0.526 V, and 0.66 respectively were reported with a dye having axial triazole based substituents on SiPcs [16]. It is well documented that MPcs based photosensitizers have excellent photoelectrochemical properties with excellent light absorption, rigid orientation of the dye on the semiconductor surface, th suitability of the position of the redox couples of the dyes are the critical factors which made them as the possible candidates as a dye in DSSCs [21]. The reports on MPcs used in DSSCs show that the metal cations in the Pc core and electron releasing/withdrawing features of the substituents, their positions, and numbers and moreover the number and type of the anchoring groups are the fundamental issues to construct efficient DSSC. Therefore, in this study, we have prepared two new SiPcs having different lengthen diaxially –COOH anchoring groups and different electron density and then their redox and electrooptical functionalities were particularly determined to show their appropriateness as synthesizers in DSSCs. Finally, these complexes were first of all investigated in DSSCs to realize good photovoltaic functionality. Here, to tailor the linker between Pc and the semiconductor surface in DSSC, bis(3-(3,5-di-tert-butyl-4-phenoxy)acrylic acid and bis((3,5-di-tert-butyl-4-phenoxy)carboxylic acid axial substituents were designed as the axial ligands of the SiPcs. Under DSSC operation, the extent of the push-pull effect, orientation of SiPcs on the electrode surface with bulky rigid linkers, the electron releasing ability of these substituents have been investigated to realize higher power conversion performance of the constructed DSSCs.

2. Experimental

2.1. Synthesis and characterization

2.1.1. Synthesis of Bis(3-(3,5-di-tert-butyl-4-phenoxy) acrylic acid) phthalocyaninato silicon (IV) (3)

After silicon phthalocyanine dichloride (**1**) (0.30 g, 4.9×10^{-4} mol) and 3,5-di-tert-butyl-4-hydroxycinnamic acid (**2**) (0.27 g, 9.8×10^{-4} mol) had been mixed in the reaction flask in the presence of dry toluene (25.0 mL) under Ar atmosphere for 15 min, sodium hydride (0.020 g, 8.3×10^{-4} mol) was added to the medium and the reaction mixture was refluxed for 36 h. The crude phthalocyanine compound obtained by evaporation of the solvent under vacuum was purified from impurities by column chromatography method in the presence of THF:EtOH (100:1) eluent system. Yield: 0.187 g (35%) Anal. calcd. For (%) $C_{66}H_{62}N_8O_6Si$ (1091.36 g/mol): C, 72.64; H, 5.73; N, 10.27; Found: C, 72.46; H, 5.29; N, 10.48; FT-IR (λ_{max}/cm^{-1}): 3389 (carboxylic O–H), 3057 (Ar–H), 2957–2879 (Aliph. C–H), 1705 (carboxylic C═O), 1615 (C═N), 1525 (C═C), 1427 (C–C), 1333 (C–N), 1074 (Si–O–C); UV–Vis (DMSO): λ_{max}/nm (10^{-6} logε, L. mol^{-1} cm^{-1}): 684 (5.22), 618 (4.67), 357 (4.94), 331 (4.96). ^{1}H NMR (500 MHz, DMSO-d_6): ppm; 11.93 (2H, s, –COOH), 9.72–9.62 (8H, m, SiPc-Ar-H), 8.56–8.46 (8H, m, SiPc-Ar-H), 8.32 (4H, s, subs-Ar-H), 6.64 (2H, d, Ar–CH═C-), 5.59 (2H, d, C═CH–COO), 1.40 (36H, s, t-BuCH_3). MALDI TOF-MS *m/z* (100%): 1091.200 $[M]^+$, 1114.260 $[M+ Na]^+$.

2.1.2. Synthesis of Bis((3,5-di-tert-butyl-4-phenoxy) carboxylic acid) phthalocyaninato silicon (IV) (5)

Silicon phthalocyanine dichloride (**1**) (0.30 g, 4.9×10^{-4} mol) and 3,5-di-tert-butyl-4-hydroxybenzoic acid (**4**) (0.24 g, 9.8×10^{-4} mol) were added in dry toluene (25.0 mL) and stirred under Ar atmosphere for 15 min. Then, sodium hydride (0.020 g, 8.3 × 10−4 mol) was added to the mixture. After 36 h of reflux, the solvent was evaporated under vacuum. The obtained crude phthalocyanine compound was purified by column chromatography in the presence of THF:EtOH (100:1) eluent system. Yield: 0.183 g (36%) Anal. calcd. For (%) $C_{62}H_{58}N_8O_6Si$ (1039.28 g/mol): C, 71.65; H, 5.63; N, 10.78; Found: C, 71.53; H, 5.82; N, 10.99; FT-IR (λ_{max}/cm^{-1}): 3500–2500 (carboxylic O–H), 3064 (Ar–H), 2985–2891 (Aliph. C–H), 1677 (carboxylic C═O), 1607 (C═N), 1527 (C═C), 1426 (C–C), 1332 (C–N), 1071 (Si–O–C); UV–Vis (DMSO): λ_{max}/nm (10^{-6} logε, L. mol^{-1} cm^{-1}): 676 (5.26), 606 (4.47), 347 (4.74). ^{1}H NMR (500 MHz, DMSO-d_6): ppm; 12.04 (2H, s, –COOH), 9.75–9.65 (8H, m, SiPc-Ar-H), 8.59–8.53 (8H, m, SiPc-Ar-H), 7.96 (4H, s, subs-Ar-H), 1.39 (36H, s, t-BuCH_3). MALDI TOF-MS *m/z* (100%): 917.95 [M-($C_6H_8O_4$)+Na]$^+$, 978.284 [M-(C_2O_4)+Na+4H]$^+$, 1039.484 $[M]^+$, 1201.432 [M+ (CHCA)-Na-3H]$^+$, 1438.369 [M+ 2(CHCA)+Na]$^+$.

2.2. Electrochemical, in situ spectroelectrochemical and photovoltaic measurements

All Electrochemical, in situ spectroelectrochemical and photovoltaic measurements were carried out by following the procedure given in the literature [17,22,23]. GCE, Pt wire, and Ag/AgCl as the working, counter, and reference electrodes were used respectively in DCM or DMSO/TBAP electrolyte during the cyclic voltammetry and square wave voltammetry measurements. Spectroelectrochemical analysis were performed by using a Pt tulle working electrode in a spectroelectrochemical thin layer quartz cell. Detail of the experimental studies are given in the supplementary information document.

2.3. DSSC measurements

DSSC measurements were carried out by following our previous study [17]. Firstly, TiO_2 paste was immobilized onto the precleaned surface of the FTO glass by the doctor-blade machine and then it is sintered at 450 °C. Then, FTO/TiO_2 electrode was treated with $TiCl_4$ to prepare TiO_2 based photoanode and finally it was sintered 450 °C. For the binding of the dyes to the FTO/TiO_2 electrode, FTO/TiO_2 photoanodes were immersed in the 0.40 mM SiPc **3** and **5**. As the cathode, another FTO glasses was coated with platisol T/SP platinum paste and sintered at 420 °C. Then The DSSC was constructed by sandwiching Pt coated FTO cathode with FTO/TiO_2/SiPcs photoelectrodes by using a spacer. Finally, iodide/triiodide-based electrolyte was filled between two electrodes of the DSSC. For photovoltaic measurements of the DSSCs, current density (J) -voltage (V) curves were recorded, and the results were evaluated to determine the current density, open circuit potential, fill factor, and efficiency of the DSSCs. The electrochemical impedance spectroscopy measurement (EIS) was carried out by Gamry Reference 600 potentiostat in the frequency region from 0.1 Hz to 100 kHz. Detail of the DSSC measurements is given in the supplementary information document.

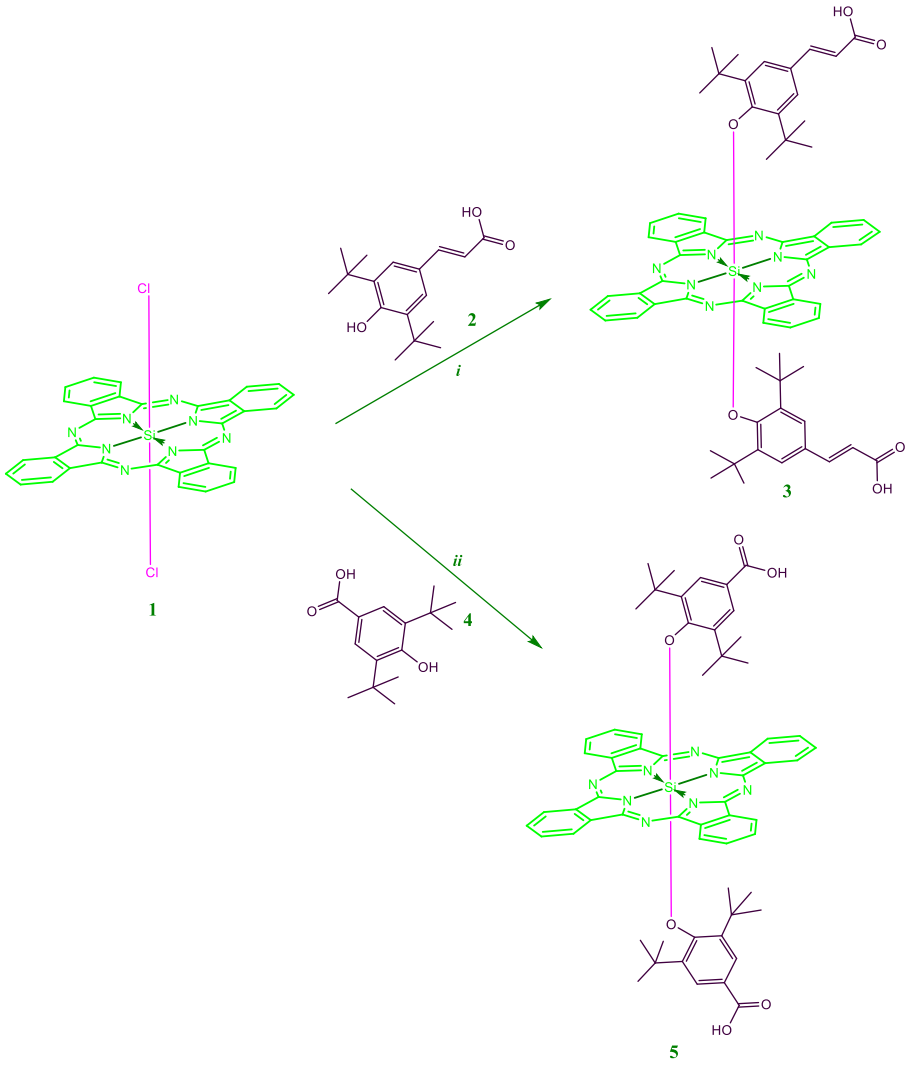

Scheme 1. Synthetic routes of the new silicon phthalocyanine; *i*: dry Toluene, dry NaH, 110 °C, 36 h, Ar atmosphere.

3. Results and discussion

3.1. Synthesis and characterization

Tert-butyl moieties containing carboxylic acid anchoring groups substituted novel diaxially silicon (IV) phthalocyanines were synthesized by mixing the compounds (**2**) and (**4**), respectively with silicon phthalocyanine dichloride (**1**) in toluene in the presence of NaH at 110 °C for 24 h under argon atmosphere (Scheme 1). The crude products obtained were purified from the column with a THF: Ethanol (100:1) solvent system using aluminum oxide filler. The synthesized SiPc complexes (**3** and **5**) were obtained in 35% and 36% yield, respectively and characterized by using ^{1}H NMR, MALDI-TOF, FT-IR, UV–Vis spectroscopy, elemental analysis and investigated the electrochemical, spectroelectrochemical and dye sensitized solar cells (DSSCs) properties.

Since the silicon phthalocyanines (**3** and **5**) have carboxyl group, carbonyl –C = O stretching peaks were observed at 1705 and 1677 cm^{-1} respectively in addition to the broad carboxyl O–H stretching peaks at around 3500-2500 cm^{-1} in FT-IR spectrum compounds. These peaks confirmed the presence of carboxyl group at the axial position. In addition, the aromatic and aliphatic C–H vibration bands were observed at 3057, 3064 cm^{-1} for SiPc **3** and between 2985 and 2879 cm^{-1} for SiPc **5**, which were compatible with the expected structures. Also, the most characteristic vibration bands at 1074 and 1071 cm^{-1} indicated the bond of Si–O–C for **3** and **5**.

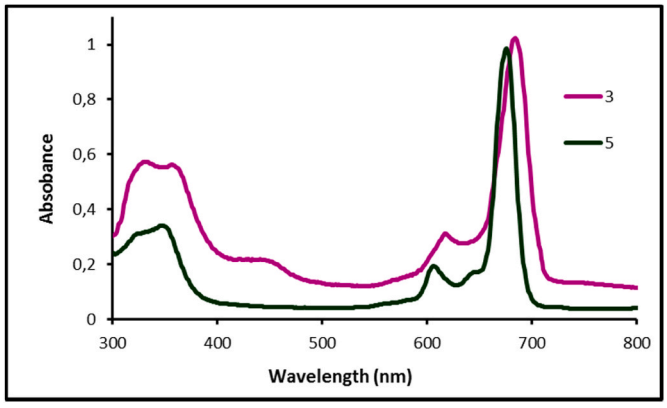

Fig. 1. UV–Vis spectra of **3** and **5** (6.0 × 10^{-6} M) in DMSO.

SiPc complexes (**3** and **5**) were also characterized with the UV–Vis spectral measurements (Fig. 1). In the absorption spectra of the newly synthesized SiPc complexes (**3** and **5**), characteristic Q bands were observed at 684 nm and 676 nm, respectively, due to the π→π* transition between the ground state HOMO (highest occupied molecular

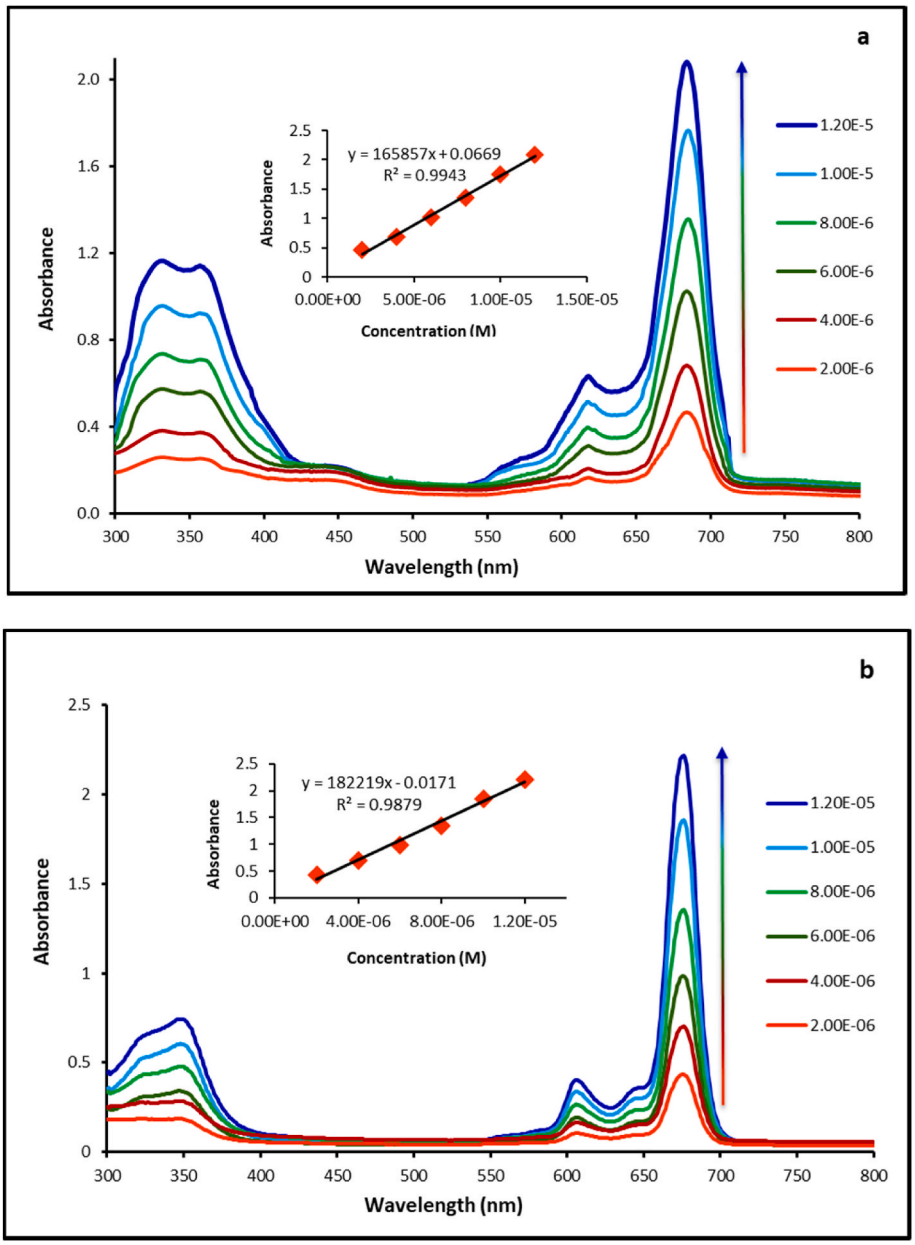

Fig. 2. UV–Vis absorption spectra of a) **3** and b) **5** in DMSO at varying concentrations.

orbital) energy level and the excited LUMO (lowest unoccupied molecular orbital) energy level. At the same time, characteristic B bands (Soret) originating from π→π* transitions were also seen between 300 and 400 nm [10,11,18–20]. The bands observed in high intensity at 684 and 676 nm, respectively, of the SiPc complexes (**3** and **5**) are the Q absorption bands belonging to the π–π* transitions of **3** and **5** in DMSO medium. A shoulder of each of the **3** and **5** pc complexes was seen at 618 and 606 nm, respectively, in the slightly higher energy part of the Q bands. (Fig. 1). When the UV–Vis spectra of complexes **3** and **5** were compared with each other, a red shift was observed in the Q band of the spectrum of complex **3** because of effect of extended conjugation [10,11, 18–20].

Also, aggregation behaviors of **3** and **5** were examined in DMSO at in 2.0x10^{-6}-1.2 × 10^{-5} M concentration range (Fig. 2). Because aggregation creates challenges in the application areas of phthalocyanines, the lack of aggregation phenomena in the solution is quite important for effective sensitization of the material. SiPc **3** and **5** do not demonstrate any aggregation in DMSO owing to axial substitution. As the concentration increased, the intensity of the Q band increases harmoniously without shifting, which shows non-aggregation of the complexes.

^{1}H NMR spectra of SiPcs (**3** and **5**) in deuterated DMSO gave a singlet at δ 11.93 and 12.04 ppm (COOH), respectively. Aromatic protons of the structures of SiPcs were observed as multiplet at δ 9.72–9.62 ppm integrating eight protons, at δ 8.56–8.46 ppm integrating eight protons for **3** and at δ 9.75–9.65 ppm integrating eight protons, at δ 8.59–8.53 ppm integrating eight protons for **5**, as expected. Substituted aromatic protons were observed as a singlet at δ 8.32 ppm for **3** and δ 7.96 ppm for **5**. Also, in the ^{1}H NMR spectrum of **3**, Ar-CH═C and C═CH–COO protons were observed as doublets at δ 6.64 ppm and 5.59 ppm, respectively. In the ^{1}H NMR spectra of compounds **3** and **5** the broad peaks at δ 1.40 and 1.39 ppm, indicated the presence of the aliphatic t-BuCH_3 protons, respectively. Final evidence of **3** and **5** were given by MALDI-TOF MS where molecular ion peaks atm/z: 1091.200 $[M]^+$, 1114.260 $[M+ Na]^+$ and 917.95 $[M-(C_6H_8O_4)+Na]^+$, 978.284 $[M-(C_2O_4)+Na+4H]^+$, 1039.484 $[M]^+$, 1201.432 $[M+(CHCA)-Na-3H]^+$, 1438.369

Table 1
Electrochemical data of the complexes in DMSO/TBAP solution. All potentials were given versus Ag/AgCl.

	$E_{1/2}$ (V) of Redox Processes							
Complexes	R(1)	R(2)	Oxd(1)[a]	Oxd(2)	[b]E_{LUMO}	[c]E_{HOMO}	E_{gap} (eV)	Ref.
SiPc 3 (DCM)	−0.48	−0.91	0.98 (0.65)	–	−3.85	−5.31	1.48	tw
SiPc 5 (DCM)	−0.44	−0.90	1.13 (0.75)	–	−3.89	−5.46	1.57	tw
SiPc 5 (DMSO)	−0.42	−0.89	1.15 (0.77)	–	−3.91	−5.48	1.57	tw
SiPc[d]	−0.90	−1.48	1.00					[41]
SiPc[e]	−0.64	−1.07	0.72	1.03				[25]
SiPc[e]	−0.66	−1.10	0.73	1.03				[25]
SiPc[e]	−0.70	−1.18	1.23	–				[20]
SiPc[e]	−0.72	−1.25	1.35	–				[20]
SiPc[f]	−1.21	−1.76	0.53	–				[42]
SiPc[e]	−0.72	−1.13	0.75	0.98				[26]
SiPc[g]	−0.48	−0.63	–	–				[43]
SiPc[e]	−0.84	–	0.55	0.95				[24]
SiPc[e]	−0.90	–	0.55	0.96				[24]
SiPc[e]	−0.83	–	0.54	0.96				[24]
SiPc[e]	−0.82	–	0.54	0.93				[24]

[a] This small wave is assigned to the aggregated species and shown in parentheses.
[b] E_{HOMO} = -4.78 +($E_{1/2}$ (Fc)-$E_{1/2}$ (Oxd(1)).
[c] E_{LUMO} = -4.78 +($E_{1/2}$ (Fc)-$E_{1/2}$ (Red(1)).
[d] E_p or $E_{1/2}$ versus reversible Ag reference electrode in DCM.
[e] E_p or $E_{1/2}$ versus SCE in DCM.
[f] E_p versus reversible Ag reference electrode in DCM.
[g] $E_{1/2}$ versus vs. Ag/AgCl in water.

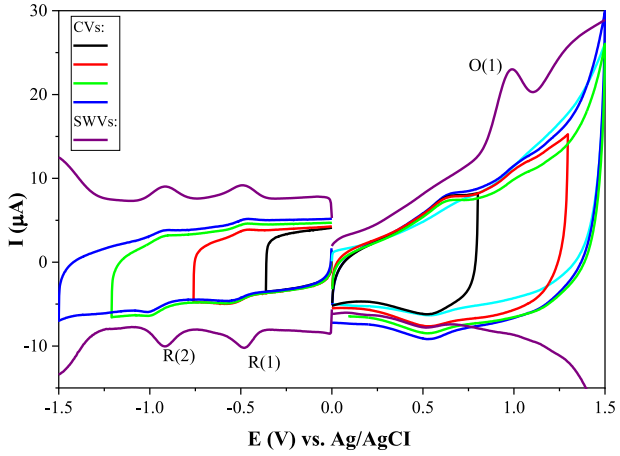

Fig. 3. CVs (recorded with different vertex potentials) and SWVs of SiPc **3** (5.0 × 10^{-4} mol dm^{-3}) recorded at 100 mVs^{-1} scan rate on a GCE working electrode in DCM/TBAP.

$[M+2(CHCA)+Na]^+$, respectively, are in accordance with the expected values. These values clearly indicate the formation of the desired products. Final evidence of **3** and **5** were given by elemental analysis and the results of the complexes are compatible with actual percentages. Consequently, all analytical data confirm that the complexes were successfully synthesized. The analysis spectra for ^{1}H NMR, FT-IR and MALDI-TOF MS (Figs. S1–S6) are presented in the supplementary material.

3.2. Voltammetric measurements

Voltammograms of SiPc **3** and **5** were recorded on GCE in DCM/TBAP and the half wave peak potentials ($E_{1/2}$) of the redox processes of the complexes are represented in Table 1. The influence of the different length and electron density of the axial ligands on SiPcs were compared with each other. As shown in, Fig. 3, two electron reversible reduction couples of the complex **3** are observed at −0.42 V (R(1)) and −0.96 V (R(2)) during the cathodic potentials. Peak analyses with respect to the

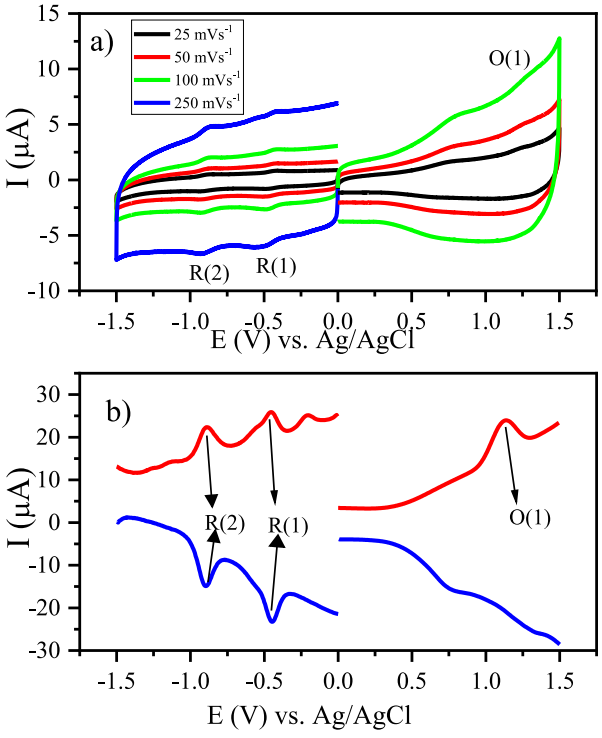

Fig. 4. CVs and SWVs of SiPc **5** (5.0 × 10^{-4} mol dm^{-3}) recorded at various scan rates on a GCE working electrode in DCM/TBAP.

cathodic to anodic peak separations (Δ*E*), changing of the ΔE with the square roof of the scan rates, Peak to peak current ratios (I_{pa}/I_{pc}) indicates the reversible character of these couples. Differently, the complex **3** does not illustrate well resolved oxidation process. Only one irreversible oxidation wave is observed at around 1.00 V (O (1)). A small wave observed at around 0.70 V may due to the chemical reaction products produced after the O(1) process. Since it is not observed during the first scan, and it is observed during the consecutive scans. SWVs illustrated in Fig. 3 support these peak behaviors.

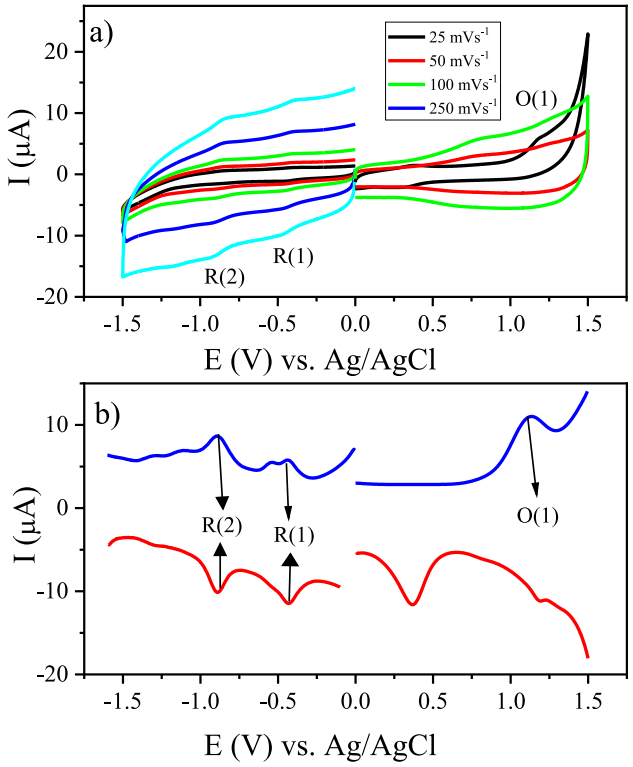

Fig. 5. CVs and SWVs of SiPc **5** (5.0×10^{-4} mol dm^{-3}) recorded at various scan rates on a GCE working electrode in DMSO/TBAP.

Fig. 4 shows the CVs and SWVs of the complex **5**. Altering the bis(3-(3,5-di-tert-butyl-4-phenoxy)acrylic acid axial ligand (on SiPc **3**) with bis((3,5-di-tert-butyl-4-phenoxy)carboxylic acid ligand (on SiPc **5**) does not considerable alter the redox responses of the complexes. Two reductions (R(1) and R(2)) and one oxidation (O(1)) processes are recorded at −0.42, −0.96 V, and 1.03 V respectively. Both SiPcs having redox inactive Si^{4+} metal centers, thus, these complexes undoubtedly illustrate only Pc based redox responses and the axial ligands on Si center do not considerably influence the redox response of the Pc ring. Note that the reduction and oxidation potentials of the complex **5** are nearly same with those of **3**. From their general shapes of the voltammograms and peak analyses, reduction waves of **5** appear to be electrochemically reversible to quasi-reversible one-electron transfers, while the oxidation wave is irreversible. SWVs support this character of the couples (Fig. 4b). The voltammetric responses of **5** are also carried out in DMSO/TBAP instead of DCM to investigate effect of the electrolyte. When the voltammograms in Figs. 4 and 5 re compared with each other, it is clearly shown that SiPc **5** illustrates completely similar redox couples at approximately similar potentials with similar reversibility in both electrolytes, which indicate that the electrolyte polarity does not considerably influence the redox features of the complexes.

When compared with the similar SiPc complexes in the literature, it is shown that the positions and general behaviors of the peaks of both SiPcs are in harmony with the SiPcs reported in the literature. For instance, Martín-Gomis et al. reported the electrochemical responses and DSSC performance of two SiPc complexes bearing formylbenzoic acid and sulfamic acid axial ligands [19]. They reported one quasi-reversible one-electron oxidation and one quasi-reversible one-electron reduction for both SiPcs in tetrahydrofuran (THF) containing 0.1 M tetrabutylammonium hexafluorophosphate (TBAPF6) electrolyte respectively. In another study, Bergkamp et al. compared the electrochemical responses of five SiPcs having different axial ligands and they reported that the first reduction process between −0.82 and −0.90 V, the first and second oxidation processes between 0.54 and 0.55 V and 0.93 and 0.96 V vs SCE in DCM/TBAP were reported respectively [24]. Bıyıklıoğlu and his coworkers studied several SiPcs and reported that these complexes generally illustrated two reduction processes between −0.60 and −1.50 V and one oxidation at around 1.0 V, which slightly varied with changing the axial ligands [20,25,26]. When all these studies are evaluated, it can be concluded that redox responses of SiPcs studied here are in harmony with the similar ones in the literate and the redox activities of SiPcs are resulted from the electron transfer processes of the Pc ring. The axial ligands slightly alter the peak positions and peak reversibility due to the influence of the electron releasing/withdrawing features and different polarity and potential windows of the electrolytes.

3.3. *In-situ spectroelectrochemical measurements*

It is well reported that Si^{4+} metal ions in the core of Pc ring have no redox activity within the potential window of the electrolytes, thus spectral responses observed during the spectroelectrochemical measurements are resulted from the redox processes of the Pc ring. Although, in-situ spectroelectrochemistry of MPcs having Pc ring-based processes are frequently reported in the literature, in-situ spectroelectrochemical characterizations of SiPcs are quite rare. Thus, the spectroelectrochemical responses of SiPc obtained here will make important contributions to the elucidation of the electrooptic applications of these complexes. Fig. 6 illustrates the spectral changes of the complex **3** observed during the electron transfer processes in DCM/TBAP electrolyte. Without a potential application, the complex **3** gives the characteristic B and Q bands at 325 and 685 nm. Under −0.60 V constant potential application (slightly higher then R(1) peak potential), two distinct spectral changes are observed as shown in Fig. 6a. This response may be due to the succeeding chemical reaction after the first reduction reaction. In the frontier part of the spectral change, while the B band increases and the Q band decreases in intensity with a shift to 670 nm, a charge transfer band is observed at 588 nm (Fig. 6a–i). The band at 588 nm is a characteristic change for a Pc based reduction process. However, the shifting of the Q band is not a common change for the Pc based reduction. It is well reported in the literature that the Q band decreases without a shift during the Pc based reduction [27–30]. However here, the Q band shifts from 685 nm to 670 nm. These unusual spectral changes may be due to the possible succeeding chemical reaction, which may be the releasing of the axial ligand during the redox reaction. In the later part of the spectral changes, the Q band continues to decrease without a shift and new charge transfer bands are observed at 440, 517, 577, and 619 nm (Fig. 6a–ii). The spectral changes during the electrolysis of the species at −0.60 V cause a color change from cyan (legend □; x = 0.2956 and y = 0.3339) to blue (legend ○; x = 0.2956 and y = 0.3339) as shown in Fig. 6d. During the second reduction reaction, while all the existing bands disappear, new distinct bands are formed at 390, 454, and 515 nm (Fig. 6b), which assign to the second Pc reduction process. These spectral changes cause to the color changes to red (legend △; x = 0.3804 and y = 0.3347) as shown in the chromaticity diagram. Fig. 6c represents the spectral changes under 1.20 V constant potential application (O(1)). Two distinct spectral changes are also observed during the oxidation of the complex due to the succeeding chemical reaction. At the beginning of the oxidation reaction, while the Q band slightly increases with a shift from 685 to 689 nm, all other bands slightly decrease in intensity. Then all bands decrease in intensity due to the decomposition of the cationic species under the applied potential. A slight color changes from cyan to blue (legend ☆; x = 0.2773 and y = 0.3165) is observed after the oxidation process as shown in Fig. 6d.

Altering the axial ligand considerably influences the spectral changes of **SiPcs** as shown in Fig. 7. Like the complex **3**, two different spectral changes are observed during the first reduction reaction of the complex **5**. However differently, while the Q band decreases with a shift for the complex **3**, it increases with a shift for the complex **5** (Fig. 7a–i). The Q band increases in intensity with a shift from 676 nm to 670 nm, while

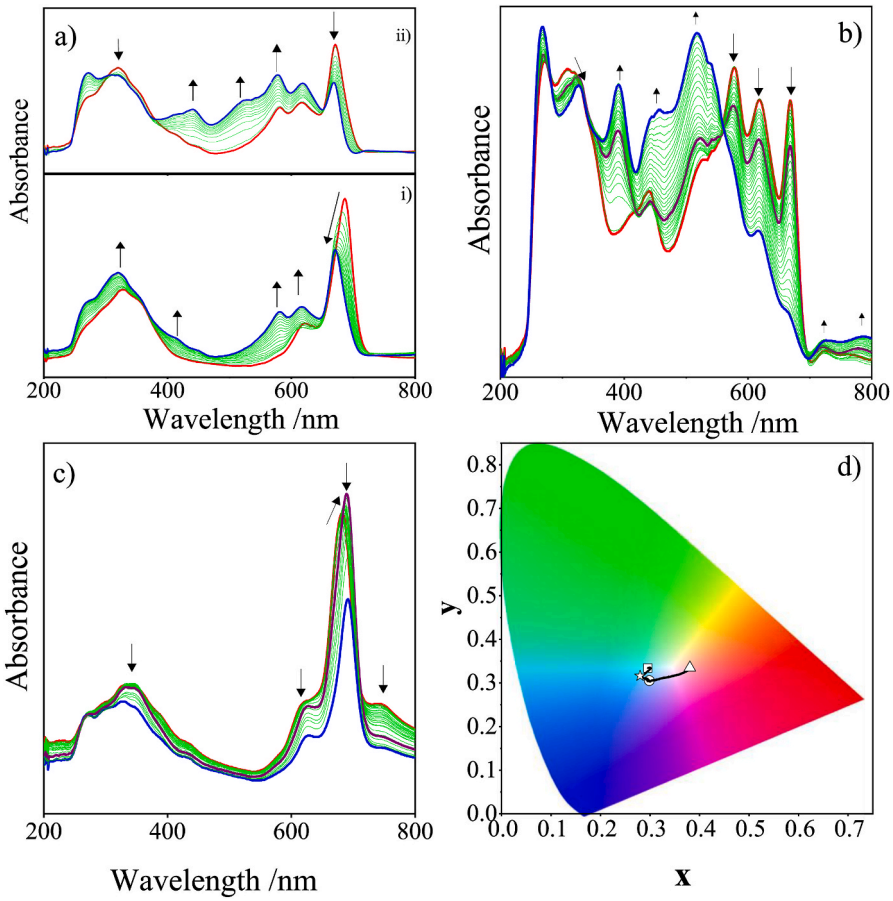

Fig. 6. In-situ UV–Vis spectral changes of SiPc **3** in DMSO/TBAP electrolyte. **a**) $E_{app} = -0.60$ V, **b**) $E_{app} = -1.30$ V, **c**) $E_{app} = 1.20$ V, **d**) Chromaticity diagram (each symbol represents the color of electro-generated species; □: $[L_2Si^{IV}Pc^{2-}]$; ○: $[L_2Si^{IV}Pc^{3-}]^{1-}$; △: $[L_2Si^{IV}Pc^{4-}]^{2-}$; ☆: $[L_2Si^{IV}Pc^{1-}]^{1+}$.

new increasing bands are observed at 400, 577, and 610 nm during the frontier spectral changes under −0.60 V applied potential as shown in Fig. 7a–i. Increase of the Q band may be due to the high molar extinction coefficient of the monoaninic form of the complex. During the later spectral changes under −0.60 V applied potential, the Q band continues to increase without a shift, while other bands also increase (Fig. 7a–ii). During the second reduction reaction, the B and Q bands decrease while a new band is observed at 483 nm due to the reduction of monoaninic SiPc to dianionic SiPc species (Fig. 7b). The complex **5** illustrates similar spectral changes with those of the complex **3** during the oxidation reaction as shown in Fig. 7c. Firstly, the Q band increases in intensity with a shift from 675 nm to 670 nm and the intensity of all other bands slightly decrease, then all bands decrease in intensity until the end of the oxidation process. The original light green color (legend □; x = 0. 0.3095 and y = 0.3521) of the complex turns to deep blue (legend ○; x = 0.1655 and y = 0.1886) and then to blue (legend △; x = 0.2211 and y = 0.227) after the reduction processes and turns to cyan (legend ☆; x = 0.2813 and y = 0.3123) after the oxidation process as shown in the chromaticity diagram (Fig. 7d). The spectroelectrochemical results of the complexes shows their superior functionality for various photoelectrochemical applications, such as electrochromic devices, photoelectrochemical systems and solar cells.

3.4. Photovoltaic properties

DSSC device constructed here consists of SiPc-sensitized FTO/TiO_2 photoanode, a Pt coated FRO counter electrode (FTO/Pt cathode) and the redox couple which fills the space between the electrodes. During the illumination of FTO/TiO_2//Pt/FTO DSSC device, the electrons in the highest occupied molecular orbital level (HOMO) level of the SiPc sensitizer are rapidly excited to the lowest unoccupied molecular orbital level (LUMO) and then they are injected into the conduction band (CB) of TiO_2. Then they are transferred to the FTO/Pt cathode through the external circuit. The holes on the HOMO of the SiPc are reduced by the redox couple, which regenerates the SiPc sensitizer. Reduction of the oxidized species are reduced at the cathode by the transferred electron from the photoanode and complete the circuit. The performance of DSSC depends on the optical absorbance of dye, positions of the HOMO and LUMO levels and such undesirable competitive phenomena, such as tendency of the recombination of the charge carriers, and possibility of the exited electron's non-radiative decay [31]. To diminish the undesirable competitive phenomena, SiPc **3** and **5** were prepared as sensitizers, which have intense optical absorbance in the UV/blue and the red/near-IR spectral regions and suitable HOMO and LUMO band positions. As shown in Fig. 1, Both SiPcs (618 and 606 nm for **3** and **5** respectively) studied here have high absorption intensity in the far visible/near-IR region, which shows suitability of these dyes to obtain high photovoltaic performance. The HOMO and LUMO positions of SiPcs were determined by using the half wave potentials of the redox couples recorded with SWVs. The E_{HOMO} and E_{LUMO} values of the SiPc **3** and **5** tabulated in Table 1 shows suitability of them as sensitizers in DSSC. As shown in Table 1, there are small differences on the HOMO and LUMO positions for **3** and **5** due to the different position of the redox couples. The LUMO energy levels of both SiPcs lie above the CB of TiO_2 (−4.2 eV) for the transferring of the excited electrons from LUMO of SiPcs to CB of TiO_2. When compared with each other, it is shown that the LUMO energy level (−3.89 eV) of SiPc **5** is slightly close to CB of TiO_2 with respect to SiPc **3** (−3.85 eV), which could facilitate electron

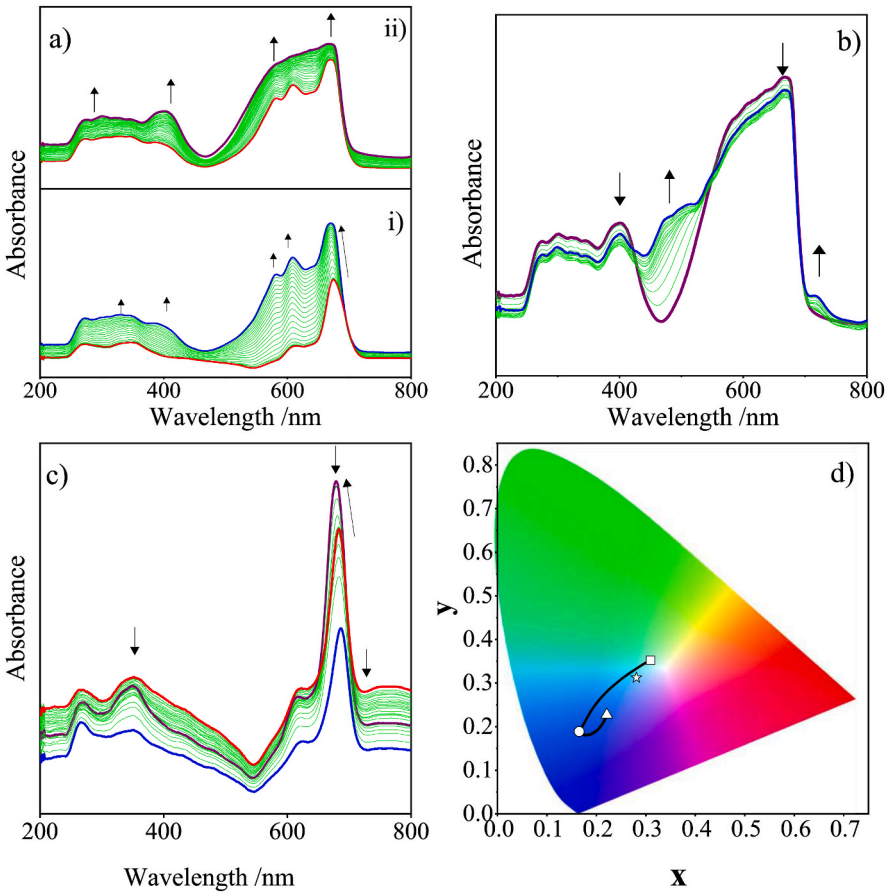

Fig. 7. In-situ UV–Vis spectral changes of SiPc **5** in DMSO/TBAP electrolyte. **a)** $E_{app} = -0.60$ V, **b)** $E_{app} = -1.30$ V, **c)** $E_{app} = 1.20$ V, **d)** Chromaticity diagram (each symbol represents the color of electro-generated species; □: $[L_2Si^{IV}Pc^{2-}]$; ○: $[L_2Si^{IV}Pc^{3-}]^{1-}$; △: $[L_2Si^{IV}Pc^{4-}]^{2-}$; ☆: $[L_2Si^{IV}Pc^{1-}]^{1+}$.

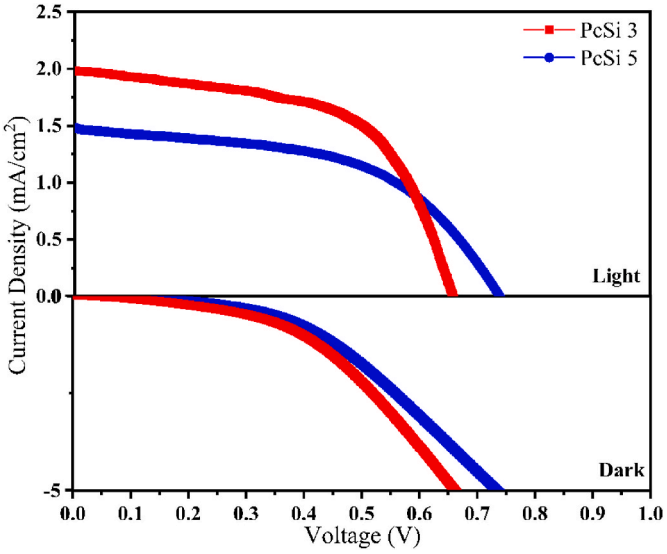

Fig. 8. J–V measurements of the DSSCs based on SiPc **3** and SiPc **5**.

transfer from the LUMO to the CB of the TiO_2. Similarly, HOMO positions of the complexes are less than that of I^-/I^{3-} couple, required for the reduction of the holes on the HOMO of the SiPcs. Like LUMO, HOMO level (−5.46 eV) of the SiPc **5** seems more favorable for the hole reduction with the I^-/I^{3-} couple ((−4.89 eV).

Photovoltaic properties of the complexes were determined by performing Current-voltage (I–V) and EIS measurements. I–V measurements of DSSCs performed under light illumination are given in Fig. 8. The basic parameters, open circuit potential (V_{OC}), the current density (J_{SC}) and FF values of the DSSC were derived from I–V curves and tabulated in Table 2. As shown in this table, photovoltaic performances of SiPc **3** and **5** are among the highest performance among the published SiPcs. Considering the fact that the HOMO–LUMO levels and the UV–vis absorption spectra for both SiPcs **3** and **5** are quite similar, the better results in the DSC performance for SiPc **5** may be attributed to the different acceptor groups and slight differences on the energy levels. In the case of SiPc **5**, the presence of a shorter linker between the complex and the anchoring carboxylic acid group increases the electron injection efficiency and improving the performance of the photovoltaic device. Although high performances with respect to photocurrent density, efficiency and fill factor values are obtained with SiPc **5** having shorter axial anchoring groups, the open circuit potential of it is less than SiPc **3**. Proximity of the electron donating Pc ring of the SiPc **3** to the TiO_2

Table 2
Photovoltaic properties of the MPc bearing DSSCs.

Dye	J_{SC} (mA/cm^2)	V_{OC} (V)	FF (%)	η (%)	Ref.
SiPc-CDCA	1.208	0.611	0.72	0.53	[20]
SiPc-CDCA	1.168	0.556	0.67	0.44	[20]
SiPc	0.55	0.41	0.58	0.16	[43]
SiPc	2.25	0.34	0.69	0.53	[19]
SiPc	3.26	0.40	0.59	0.77	[19]
SiPc 3	**1.48**	**0.751**	**0.52**	**0.57**	**tw**
SiPc 5	**1.99**	**0.657**	**0.57**	**0.75**	**tw**
N719	**19.10**	**0.721**	**0.66**	**9.14**	**tw**

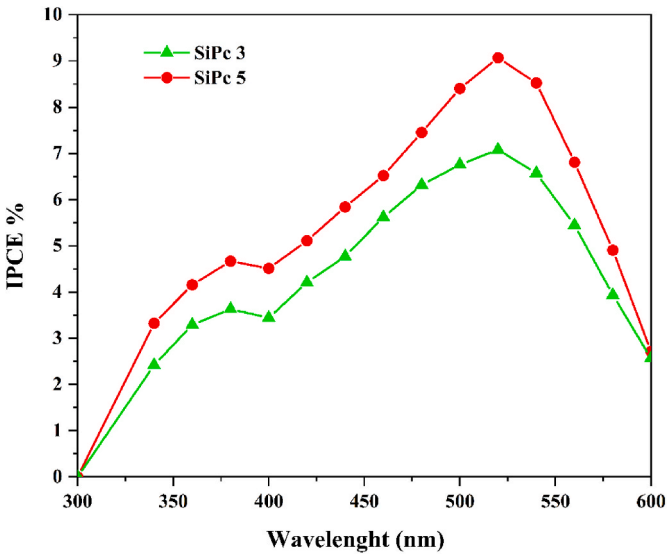

Fig. 9. IPCE plots of the DSSCs based on SiPc **3** and SiPc **5**.

semiconductor due to the short linker in turn increases the carrier mobility and enhances the DSSCs performance. Consequently, enhanced performances of SiPc **5** influence the photovoltaic efficiency, thus SiPc **5** (0.75%) show higher efficiency than SiPc **3** (0.57%).

The strong binding of SiPcs to the TiO_2 semiconductor with carboxyl anchoring groups, well orbital overlapping with the short linkers, and the close orientation of the conjugated Pc rings of the SiPcs with the rigid 3,5-di-tert-butyl-4-phenoxy axial spacer to the TiO_2 surface facilitate the electron transfer process from dyes to the semiconductor, which enhance the DSSC performance [31]. The influence of the linker to the DSSC was well introduced by Torres et al. They reported that flexible and non-directional linkers caused decreasing of the efficiency of the DSSCs. They reported efficiencies of 3.52, 3.10, 2.20, 0.67, and 0.4% with no spacer, vinyl, phenyl, phenyl, and phenoxy linkers on the unsymmetrical zinc phthalocyanines bearing an anchoring carboxylic anchoring groups respectively [32]. In addition to the different length of the anchoring group, the so-called "push-pull" effect of the substituents also influence the performance of the DSSCs. Due to the electron-withdrawing feature of COOH anchoring group and the electron-donor character of the 3,5-di-tert-butyl-4-phenoxy axial chains of SiPcs have ability to facilitate the electron injection from LUMO of SiPcs to the CB of TiO_2. Moreover, the alkene functionality on the anchoring group of the SiPc **3** may increase the push-pull effect due to the higher π electrons, thus have tendency to influence electron transfer functionality. Additionally, π electron density of the complex dominantly influences the HOMO energy level of dyes. Thus, the higher V_{OC} value of SiPc **3** can be attributed to the destabilized HOMO of SiPc **3** (−5.31 eV) compared to SiPc **5** (−5.46 eV). Position of the HOMO level of dyes is another key factor for the efficient regeneration of the dye with the I^-/I^{3-} couple in the electrolyte. Lying of the HOMO of SiPc **3** and SiPc **5** below the reduction potential of the I^-/I^{3-} couple (−4.89 eV) shows suitability of these dyes for this issue for the efficient completion of the DSSC circuit.

The higher performances of SiPc studied here than many similar examples (some are listed in Table 1) in the literature may be due to the bulky axial ligands which have high push-pull effect due to high electron density and high solubility in various solvents. As well reported in the literature, axial substitutions on Pcs were generally preferred to decrease the aggregation of the dyes and close orientation of dyes on the surface of the semiconductors. For example, Torres and co-workers reported DSSC performance of titanium(IV) phthalocyanines with the carboxylic acid (0.2% of efficiency) and sulfonate (0.14% of efficiency) axial anchoring groups and they realized that their efficiencies are very low due to poor electron injection despite the strongly adsorption of dyes onto the TiO_2 surface [33,34]. In another study, Sastre-Santos et al. tested two different Si (IV) phthalocyanine derivatives bearing axial terephthalic and two 4′-carboxyphenylcyanoacrylic moieties and reported 0.53 and 0.77% of efficiency ang high V_{OC} due to the high electron-withdrawing feature of the cyanoacrylic anchoring groups [19].

To support the J-V responses, incident photon-to-current responses of the DSSCs are recorded to determine incident photon-to-current efficiency (IPCE) of the dyes (Fig. 9). The incident photon-to-current conversion efficiency (IPCE) is calculated by dividing the number of produced electrons by the number of incident photons. While N719 has an incident photon-to-current efficiency (IPCE) of approximately 80% at $\lambda = 535$ nm, the SiPc **3** and SiPc **5** dyes have IPCE values of 7.10% and 9.15% respectively.

To further examine the photovoltaic performance of the SiPc based DSSCs during the operations, EIS analysis of DSSCs were carried at the open-circuit voltage of the DSSC under light illumination and their Nyquist and Bode plots are analyzed to derive the basic EIS parameters. The Nyquist plots of DSSCs (Fig. 10a) their equivalent circuit and Bode plots (Fig. 10b) are evaluated to determine the conductivities and electron lifetimes. As shown in Fig. 10a, there are two semicircles in the Nyquist plots in the high and middle frequency regions. Inset in Fig. 10a show the Randles-Sevcik equivalent circuit indicating series resistance (Rs), charge transfer resistances at the cathode (R_{CT1}) and photoanode (R_{CT2}). R_{CT1} of the reaction of I^-/I_3^- process at the counter electrode was evaluated by using the small loop in the high frequency region [35,36]. The R_{CT2} between TiO_2/SiPc and/I^-/I_3^- redox couple interfaces was

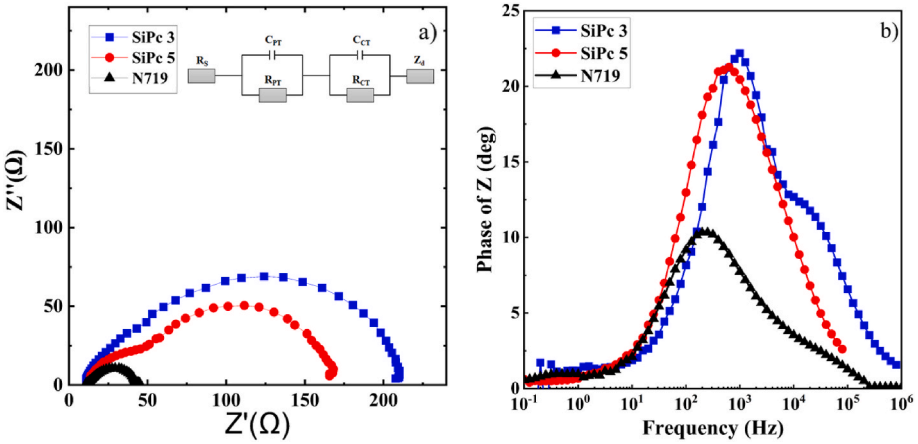

Fig. 10. a) Nyquist plots and **b**) Bode plots of the DSSCs based on SiPc **3**, SiPc **5** and N719.

Table 3
Equivalent circuit parameters of the DSSCs according to electrochemical impedance spectroscopy.

Dye	$R_S(\Omega)$	$R_{CT1}(\Omega)$	R_{CT2} (Ω)	f_{max} (Hz)	τ_e (ms)
SiPc 3	10.89	43.9	163.1	1000	0.16
SiPc 5	12.6	45.4	120.3	630.95	0.25
N719	10.44	19.07	15.58	196.64	0.81

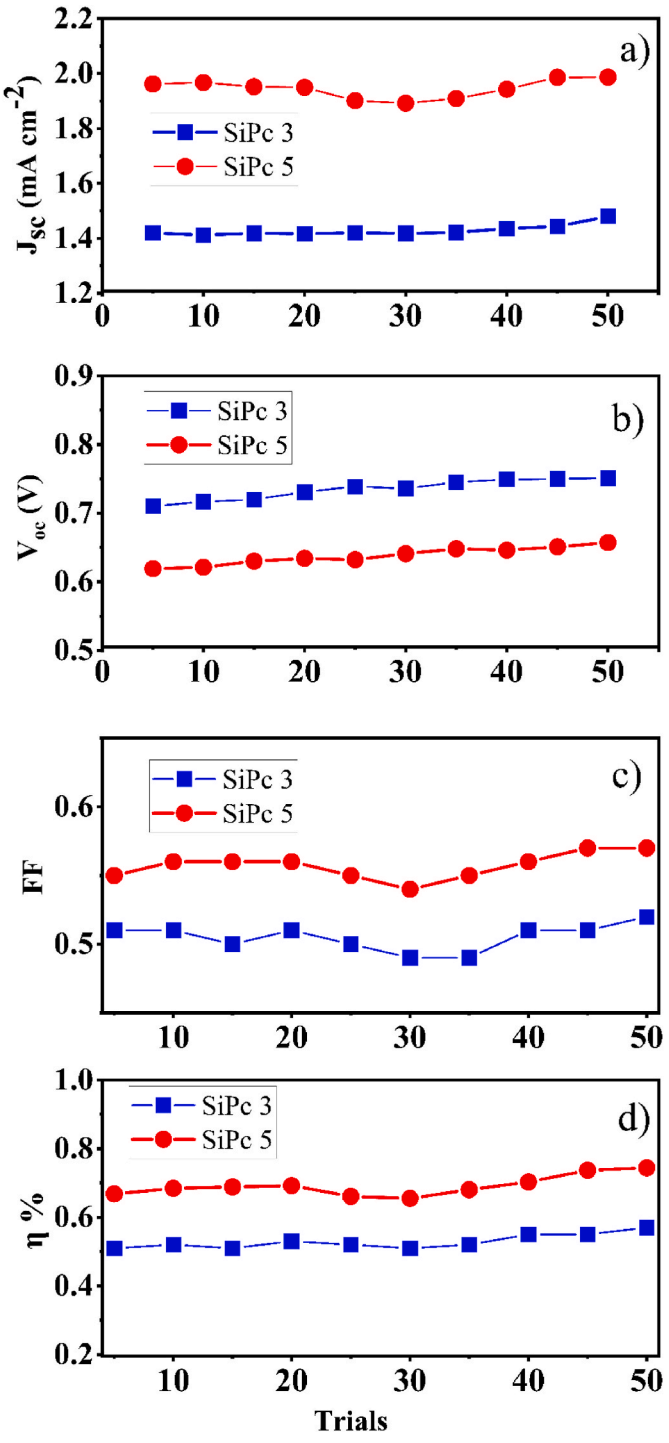

Fig. 11. Stability tests of photovoltaic cells of SiPc **3** and SiPc **5** derived from continuous 50 LSVs under the illumination with one sun.

derived from the large loop in the middle frequency region [37]. Generally, the charge transfer resistance (R_{CT2}) between TiO_2/SiPc and/I^-/I_3^- redox couple interfaces is more dominant on the efficiencies of the cell. As shown in Tables 2 and 3, the photovoltaic performance differences are in harmony with the charge transfer resistance of the complexes. The small radius of the major semicircle of SiPc **5** is lower than that of SiPc 3 due to the low R_{CT2} of the SiPc **5** (120.3 **Ω**), which is consistent with its high photocurrent density responses [35,36]. A decrease in the R_{CT2} shows decelerating the charge carrier recombination, which reflect higher photocurrent density of the photoelectrodes [38]. Sifting of the frequency of the phase shift towards the lower value also support the photocurrent and the R_{CT2} responses of the cells. The phase angles of the cells are considerably less than that of the ideal capacitors (less than 90°) due to the pseudo capacitances of the TiO_2/-SiPc electrodes instead of an ideal capacitor. This pseudo capacitances of the TiO_2/SiPc electrodes are also confirmed by the capacitance elements of the equivalent c Fig. 10a [39]. In addition to the R_{CT2} responses, different electron lifetime (τ_e) of the exited electrons during the operation of DSSCs (calculated using the equation $\tau_e = 1/2\pi f$) can be also used as an indicator for the different performances. The high electron lifetime cause to increase efficiency of the electron transfer process so consequently increase the solar cell photovoltaic efficiency. The EIS results recorded here clearly show that the longer electron lifetime in case of SiPc **5** (0.25 ms) with respect to SiPc **3** (0.16 ms) is in harmony with its higher photovoltaic performance.

3.5. Stability measurements in DSSC

The two most significant criteria for commercial applications of DSSCs are efficiency and stability. The total stability of DSSCs is highly influenced by the stability of their cell components, which include the dye, electrolyte, PE, and CE. As a result, the stability of each cell component is critical for their practical application. Fig. 11 presents the photovoltaic data of the DSSC during aging at room temperature with one sun illumination. The performance of SiPc **3** was remarkably stable over. At the end of the 50th trials, Voc of the cell consisting of SiPc **3** increases 0.04 V. The efficiency of the cell slightly increases at the end of the 50th trials under light soaking as shown in Fig. 11. Increasing the Voc as 0.04 V and Jsc as 0.03 mA cm^{-2} are also observed with The SiPc **5**, thus FF of the cell increases 5% at the end of the 50th trial.

It is well-known that R_s, R_{ct1}, R_{ct2} and electron lifetime are the key parameters evaluating the stability of DSSCs. Fig. 12 shows the impedance spectroscopy of the first trial and fifth trial under room temperature in 1 sun for SiPc **3** and SiPc **5** respectively. For both SiPc dyes, the middle frequency peak slightly shifts towards the higher frequency in the Bode phase plots which means that the electron lifetime decreases for the increasing trial in a very small way. The growth in the radius of the low-frequency region in the Nyquist plot indicates that diffusion resistance increases during trials, most likely due to a decrease in triiodide concentration produced by impurity reaction [40].

4. Conclusion

Using a tetravalent Si $^{4+}$ central in the Pc core and different lengthened axial ligands were the main motivation for the synthesis new dyes for DSSCs. For these hypothesis, two new SiPcs bearing bis(3-(3,5-di-tert-butyl-4-phenoxy)acrylic acid axial ligand (on complex **3**) and bis ((3,5-di-tert-butyl-4-phenoxy)carboxylic acid ligand (on complex **5**) axial ligands were synthesized. Although SiPc were unsubstituted at the peripheral and nonperipheral positions, axial substituents considerably increased their solubility in polar DMSO and nonpolar DCM media. The better solubility of the complexes opens new way for their potential usage in various electrochemical technologies. To predict their potential usages, voltammetric and spectroelectrochemical analysis were performed. The results indicated that, axial ligands did not considerable influenced the voltammetric responses. Both SiPcs were tested as

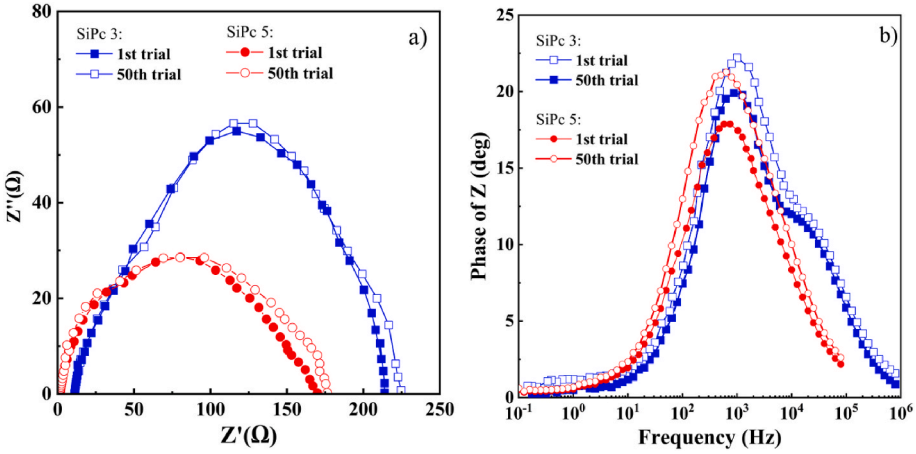

Fig. 12. EIS responses of SiPc **3** and SiPc **5** during first and 50. cycles. **a**) Nyquist plots and **b**) Bode plots.

potential dyes in DSSCs. The higher open circuit potential of the SiPc **3** were obtained due to high π electron density on the axial ligands. The shorter linker between Si center and carboxyl anchoring groups of the SiPc **5** enhanced the photocurrent density and fill factor which directly influenced the photovoltaic efficiency of the complex. The higher performances of SiPc studied here than many similar examples in the literature may be due to the bulky axial ligands which had high electron density and high solubility in various solvents.

CRediT authorship contribution statement

Gülşah Gümrükçü Köse: Conceptualization, Methodology, Supervision, Synthesis, Characterization, Investigation, Validation, Formal analysis, Data curation, Visualization, Writing – original draft, Writing – review & editing, critically for important intellectual content. **Gülnur Keser Karaoğlan:** Synthesis, Characterization, Investigation, Validation, Formal analysis, Data curation, Visualization, Writing – original draft, Writing – review & editing, critically for important intellectual content. **Yaren Erdağ Maden:** Visualization, Investigation. **Atıf Koca:** Conceptualization, Methodology, Supervision, Investigation, Validation, Formal analysis, Data curation, Visualization, Writing – original draft, Writing – review & editing, critically for important intellectual content.

Declaration of competing interest

The authors declare that they have no known competing financial interests or personal relationships that could have appeared to influence the work reported in this paper.

Data availability

No data was used for the research described in the article.

Acknowledgments

This work was supported by Yildiz Technical University (Project No. FBA-2021-4489), Marmara University BAPKO (FYL-2022-10414). Atıf Koca thanks Turkish Academy of Sciences (TUBA) for support.

Appendix A. Supplementary data

Supplementary data to this article can be found online at https://doi.org/10.1016/j.dyepig.2022.110686.

References

[1] Alsudairi A, Li J, Ramaswamy N, Mukerjee S, Abraham K, Jia Q. Resolving the iron phthalocyanine redox transitions for ORR catalysis in aqueous media. J Phys Chem Lett 2017;8:2881–6. https://doi.org/10.1021/acs.jpclett.7b01126.
[2] Koca A. Copper phthalocyanine complex as electrocatalyst for hydrogen evolution reaction. Electrochem Commun 2009;11:838–41. https://doi.org/10.1016/j.elecom.2009.02.001.
[3] Ozoemena KI, Nyokong T. Novel amperometric glucose biosensor based on an ether-linked cobalt (II) phthalocyanine–cobalt (II) tetraphenylporphyrin pentamer as a redox mediator. Electrochim Acta 2006;51:5131–6. https://doi.org/10.1016/j.electacta.2006.03.055.
[4] Mani V, Devasenathipathy R, Chen SM, Huang ST, Vasantha V. Immobilization of glucose oxidase on graphene and cobalt phthalocyanine composite and its application for the determination of glucose. Enzym Microb Technol 2014;66:60–6. https://doi.org/10.1016/j.enzmictec.2014.08.009.
[5] Lin CL, Lee CC, Ho KC. Spectroelectrochemical studies of manganese phthalocyanine thin films for applications in electrochromic devices. J Electroanal Chem 2002;524:81–9. https://doi.org/10.1016/S0022-0728(02)00757-X.
[6] Solis C, Baigorria E, Milanesio ME, Morales G, Durantini EN, Otero L, Gervaldo M. Electrochemical polymerization of EDOT modified Phthalocyanines and their applications as electrochromic materials with green coloration, and strong absorption in the Near-IR. Electrochim Acta 2016;213:594–605. https://doi.org/10.1016/j.electacta.2016.07.086.
[7] Garcia-Iglesias M, Yum JH, Humphry-Baker R, Zakeeruddin SM, Péchy P, Vázquez P, Palomares E, Grätzel M, Nazeeruddin MK, Torres T. Effect of anchoring groups in zinc phthalocyanine on the dye-sensitized solar cell performance and stability. Chem Sci 2011;2:1145–50. https://doi.org/10.1039/C0SC00602E.
[8] Sarker AK, Kang MG, Hong JD. A near-infrared dye for dye-sensitized solar cell: catecholate-functionalized zinc phthalocyanine. Dyes Pigments 2012;92:1160–5. https://doi.org/10.1016/j.dyepig.2011.07.002.
[9] Tunç G, Güzel E, Şişman İ, Ahsen V, Cardenas-Jiron G, Gürek AG. Effect of new asymmetrical Zn (II) phthalocyanines on the photovoltaic performance of a dye-sensitized solar cell. New J Chem 2019;43:14390–401. https://doi.org/10.1039/C9NJ02585E.
[10] Amao Y, Komori T. Dye-sensitized solar cell using a TiO_2 nanocrystalline film electrode modified by an aluminum phthalocyanine and myristic acid coadsorption layer. Langmuir 2003;19:8872–5. https://doi.org/10.1021/la035001u.
[11] Komori T, Amao Y. Dye-sensitized solar cell with the near-infrared sensitization of aluminum phthalocyanine. J Porphyr Phthalocyanines 2003;7:131–6. https://doi.org/10.1142/S1088424603000185.
[12] Yu L, Fan K, Duan T, Chen X, Li R, Peng T. Efficient panchromatic light harvesting with co-sensitization of zinc phthalocyanine and bithiophene-based organic dye for dye-sensitized solar cells. ACS Sustainable Chem Eng 2014;2:718–25. https://doi.org/10.1021/sc400532g.
[13] Siddique SA, Arshad M, Naveed S, Mehboob MY, Adnan M, Hussain R, Ali B, Siddique MBA, Liu X. Efficient tuning of zinc phthalocyanine-based dyes for dye-sensitized solar cells: a detailed DFT study. RSC Adv 2021;11:27570–82. https://doi.org/10.1039/D1RA04529F.
[14] Urbani M, Ragoussi ME, Nazeeruddin MK, Torres T. Phthalocyanines for dye-sensitized solar cells. Coord Chem Rev 2019;381:1–64. https://doi.org/10.1016/j.ccr.2018.10.007.
[15] Harmandar K, Granados-Tavera K, Gezgin M, Nebioğlu M, Şişman İ, Cárdenas-Jirón G, Atilla D, Gürek AG. A new sterically hindered asymmetric zinc phthalocyanine as an efficient sensitizer for dye-sensitized solar cells. New J Chem 2022;46:714–25. https://doi.org/10.1039/D1NJ04441A.
[16] Güzel E. Dual-purpose zinc and silicon complexes of 1, 2, 3-triazole group substituted phthalocyanine photosensitizers: synthesis and evaluation of photophysical, singlet oxygen generation, electrochemical and photovoltaic properties. RSC Adv 2019;9:10854–64. https://doi.org/10.1039/C8RA10665G.

[17] Karaoğlan GK, Hışır A, Maden YE, Karakuş MÖ, Koca A. Synthesis, characterization, electrochemical, spectroelectrochemical and dye-sensitized solar cell properties of phthalocyanines containing carboxylic acid anchoring groups as photosensitizer. Dyes Pigments 2022:110390. https://doi.org/10.1016/j.dyepig.2022.110390.

[18] Amao Y, Yamada Y, Aoki K. Preparation and properties of dye-sensitized solar cell using chlorophyll derivative immobilized TiO_2 film electrode. J Photochem Photobiol Chem 2004;164:47–51. https://doi.org/10.1016/j.jphotochem.2003.11.011.

[19] Martín-Gomisa L, Barea EM, Fernández-Lázaroa F, Bisquert J, Sastre-Santos Á. Dye sensitized solar cells using non-aggregated silicon phthalocyanines. J Porphyr Phthalocyanines 2011;15:1004–10. https://doi.org/10.1142/S1088424611003914.

[20] Güzel E, Baş H, Biyiklioglu Z, Şişman İ. Dye-sensitized solar cells using silicon phthalocyanine photosensitizers with pyridine anchor: preparation, evaluation of photophysical, electrochemical, and photovoltaic properties. Appl Organomet Chem 2021;35:1–10. https://doi.org/10.1002/aoc.6214.

[21] Li X, Wang H, Wu H. Phthalocyanines and their analogs applied in dye-sensitized solar cell. In: Jiang J, editor. Functional phthalocyanine molecular materials. Springer-Verlag Berlin Heidelberg; 2010. p. 229–73. https://doi.org/10.1007/978-3-642-04752-7.

[22] Sevim AM, Arıkan S, Koca A, Gül A. Synthesis and spectroelectrochemistry of new phthalocyanines with ester functionalities. Dyes Pigments 2012;92:1114–21. https://doi.org/10.1016/j.dyepig.2011.07.015.

[23] Karadağ S, Bozoğlu C, Şener MK, Koca A. Synthesis and electrochemical properties of a double-decker lutetium (III) phthalocyanine bearing electropolymerizable substituents on non-peripheral positions. Dyes Pigments 2014;100:168–76. https://doi.org/10.1016/j.dyepig.2013.09.005.

[24] Bergkamp JJ, Sherman BD, Mariño-Ochoa E, Palacios RE, Cosa G, Moore TA, Gust D, Moore AL. Synthesis and characterization of silicon phthalocyanines bearing axial phenoxyl groups for attachment to semiconducting metal oxides. J Porphyr Phthalocyanines 2011;15:943–50. https://doi.org/10.1142/S1088424611003847.

[25] Bıyıklıoğlu Z. Water-soluble axially disubstituted non-aggregated silicon phthalocyanines and their electrochemical properties. Dyes Pigments 2013;99:59–66. https://doi.org/10.1016/j.dyepig.2013.04.017.

[26] Bıyıklıoğlu Z. Non-aggregated and water soluble amphiphilic silicon phthalocyanines with two axial substituents and their electrochemical properties. Polyhedron 2013;63:1–8. https://doi.org/10.1016/j.poly.2013.07.009.

[27] Koca A. Spectroelectrochemistry of phthalocyanines. In: Zagal JH, Bedioui F, editors. Electrochemistry of N4 macrocyclic metal complexes. Switzerland: Springer International Publishing; 2016. p. 135–200. https://doi.org/10.1007/978-3-319-31332-0_4.

[28] Dmitrieva E, Sturtz BW, Yang Y, Zhang P, Dunsch L, Kenney ME. An in situ spectroelectrochemical study of the dimeric phthalocyanines $[(SiPc)_2O][OSiHx_3]_2$, $[(SiPc)_2O][OSiHx_3]_2^+$, and $[(SiPc)_2O][OSiHx_3]_2^{2+}$. Electrochem Commun 2021;128:107048. https://doi.org/10.1016/j.elecom.2021.107048.

[29] Shiina Y, Kage Y, Furukawa K, Wang H, Yoshikawa H, Furuta H, Kobayashi N, Shimizu S. TTF-annulated silicon phthalocyanine oligomers and their external-stimuli-responsive orientational ordering. Angew Chem 2020;132:22910–8. https://doi.org/10.1002/anie.202011025.

[30] Doane TL, Chuang CH, Chomas A, Burda C. Photophysics of silicon phthalocyanines in aqueous media. ChemPhysChem 2013;14:321–30. https://doi.org/10.1002/cphc.201200962.

[31] Martín-Gomis L, Fernández-Lázaro F, Sastre-Santos Á. Advances in phthalocyanine-sensitized solar cells (PcSSCs). J Mater Chem 2014;2:15672–82. https://doi.org/10.1039/C4TA01894J.

[32] Cid JJ, García-Iglesias M, Yum JH, Forneli A, Albero J, Martínez-Ferrero E, Vázquez P, Grätzel M, Nazeeruddin MK, Palomares E, Torres T. Structure-function relationships in unsymmetrical zinc phthalocyanines for dye-sensitized solar cells. Chem Eur J 2009;15:5130–7. https://doi.org/10.1002/chem.200801778.

[33] Palomares E, Martínez-Díaz MV, Haque SA, Torres T, Durrant JR. State selective electron injection in non-aggregated titanium phthalocyanine sensitised nanocrystalline TiO_2 films. Chem Commun 2004;18:2112–3. https://doi.org/10.1039/B407860H.

[34] Rodríguez-Morgade MS, Pellejà L, Torres T, Palomares E. Ti (IV) phthalocyanines for dye sensitized solar cells. J Porphyr Phthalocyanines 2013;17:814–20. https://doi.org/10.1142/S1088424613500454. 08n09.

[35] Dou Y, Wu F, Fang L, Liu G, Mao C, Wan K, Zhou M. Enhanced performance of dye-sensitized solar cell using Bi_2Te_3 nanotube/ZnO nanoparticle composite photoanode by the synergistic effect of photovoltaic and thermoelectric conversion. J Power Sources 2016;307:181–9. https://doi.org/10.1016/j.jpowsour.2015.12.113.

[36] Ilgün C, Sevim AM, Çakar S, Özacar M, Gül A. Novel Co and Zn-phthalocyanine dyes with octa-carboxylic acid substituents for DSSCs. Sol Energy 2021;218:169–79. https://doi.org/10.1016/j.solener.2021.02.042.

[37] Cakar S, Özacar M. The pH dependent tannic acid and Fe-tannic acid complex dye for dye sensitized solar cell applications. J Photochem Photobiol Chem 2019;371:282–91. https://doi.org/10.1016/j.jphotochem.2018.11.030.

[38] Xu J, Yang W, Chen R. The photovoltaic performance of highly asymmetric phthalocyanine-sensitized brookite-based solar cells. Optik 2020;200:163413. https://doi.org/10.1016/j.ijleo.2019.163413.

[39] Chindeka F, Mashazi P, Britton J, Oluwole DO, Mapukata S, Nyokong T. Fabrication of dye-sensitized solar cells based on push-pull asymmetrical substituted zinc and copper phthalocyanines and reduced graphene oxide nanosheets. J Photochem Photobiol Chem 2020;399:112612. https://doi.org/10.1016/j.jphotochem.2020.112612.

[40] Wheeler BL, Nagasubramanian G, Bard AJ, Schechtman LA, Kenney ME. A silicon phthalocyanine and a silicon naphthalocyanine: synthesis, electrochemistry, and electrogenerated chemiluminescence. J Am Chem Soc 1984;106:7404–10. https://doi.org/10.1021/ja00336a019.

[41] Mezza TM, Armstrong NR, Ritter II GW, Iafalice JP, Kenney ME. Electrochemical studies on stacked-ring silicon phthalocyanines. J Electroanal Chem Interfacial Electrochem 1982;137:227–37. https://doi.org/10.1016/0022-0728(82)80038-7.

[42] Masilela N, Idowu M, Nyokong T. Photophysical, photochemical and electrochemical properties of water soluble silicon, titanium and zinc phthalocyanines. J Photochem Photobiol Chem 2009;201:91–7. https://doi.org/10.1016/j.jphotochem.2008.10.009.

[43] Lin KC, Doane T, Wang L, Li P, Pejic S, Kenney ME, Burda C. Laser spectroscopic assessment of a phthalocyanine-sensitized solar cell as a function of dye loading. Sol Energy Mater Sol Cells 2014;126:155–62. https://doi.org/10.1016/j.solmat.2014.03.025.